





Isotropic behavior of oxygen vibrations in PbTiO₃ investigated by Ti $L_{2,3}$ -edge electron energy-loss spectroscopy

I-C. Lin , M. Haruta ,* T. Nemoto , and H. Kurata 

Institute for Chemical Research, Kyoto University, 611-0011 Uji, Kyoto, Japan



(Received 12 March 2024; accepted 20 June 2024; published 2 July 2024)

The difference in the thermal vibration of oxygen in the cubic perovskites PbTiO₃ and SrTiO₃ was explored by associating it with their phase transitions at low temperatures. The thermal vibration factor for oxygen in cubic PbTiO₃ was estimated by employing an indirect approach that combines experimental Ti $L_{2,3}$ -edge electron energy-loss spectroscopy and crystal field multiplet calculations incorporating atomic vibrations. The results uncovered relatively isotropic vibration behavior in PbTiO₃ and strong anisotropy in SrTiO₃, despite their identical lattice parameters at different temperatures. Specifically, similar vibration factors along the Ti-O bond were estimated for both materials, whereas the amplitude of oxygen vibration in the A-O plane for PbTiO₃ was significantly smaller than that for SrTiO₃. This larger oxygen vibration in the A-O plane of SrTiO₃ can be attributed to the existence of the rotational phonon mode, contributing to a TiO₆ octahedron rotational phase transition at low temperature due to softening of the R_{25} mode. Therefore, the smaller vibration amplitude for oxygen in PbTiO₃ could possibly be attributed to the intrinsic small rotational phonon mode, leading to a zone-center displacement-type phase transition induced by a softened Γ_{15} mode. Further, the charge density map obtained by density functional theory calculation proposes a broader valence electron distribution for Pb²⁺ compared to Sr²⁺ and greater electron repulsion between Pb and O, potentially contributing to smaller oxygen vibration in the Pb-O plane of PbTiO₃. This research provides valuable insights into the role of vibrational behavior in phase transition mechanisms, and offers the potential to predict the phase transition types for perovskites in the high-temperature cubic paraelectric phase.

DOI: [10.1103/PhysRevB.110.035109](https://doi.org/10.1103/PhysRevB.110.035109)

I. INTRODUCTION

Perovskite-type oxide materials often possess useful properties such as piezoelectricity and ferroelectricity, making them widely applicable in electronic devices. Notably, titanium-based perovskite oxides such as CaTiO₃, SrTiO₃, BaTiO₃, and PbTiO₃ exhibit paraelectricity with a cubic structure ($Pm\bar{3}m$) above the Curie temperature T_C (1634 K [1], 110 K [2], 396 K [3], and 763 K [4], respectively). However, they display distinct material properties at lower temperatures due to having different phase transition types. The tolerance factor (t) based on ionic radius is often used to predict the distortion of the perovskite structure and the resulting properties [5]. Based on this factor, CaTiO₃ ($t = 0.97$), SrTiO₃ ($t = 1$), BaTiO₃ ($t = 1.09$), and PbTiO₃ ($t = 1.03$) are expected to have orthorhombic, cubic, tetragonal, and tetragonal phases, respectively. In particular, tetragonal phase ($P4mm$) BaTiO₃ and PbTiO₃ are displacive-type ferroelectric materials, and related materials such as PbZr_{1-x}Ti_xO₃ have been widely investigated and used in piezoelectric devices. Previous investigations into the origins of ferroelectricity in PbTiO₃ have focused on the density of states (DOS) and charge density distribution [6–12] in the tetragonal phase. The tetragonal distortion in PbTiO₃ enhances the hybridization between the Ti $3d$ and oxygen $2p$ states, fostering robust covalent

bonding between Ti and O atoms. In addition, theoretical [6] and experimental [8] evidence suggests that the strong ferroelectricity observed in tetragonal PbTiO₃ arises from Pb-O hybridization, contrasting with the predominantly ionic nature of Pb-O bonds in the paraelectric cubic phase.

The fundamental mechanism behind the phase transitions in these materials is attributed to soft mode phonon behavior [13]. SrTiO₃ shows an octahedron rotational phase transition in the tetragonal phase ($I4/mcm$) below T_C due to the softening of the R_{25} phonon mode [2,14,15]. While SrTiO₃ does not exhibit ferroelectricity at low temperatures, it demonstrates quantum paraelectricity due to the zero-point oscillation of phonons [16]. In contrast, both BaTiO₃ and PbTiO₃ undergo a zone-center displacive-type phase transition from the paraelectric cubic phase to a ferroelectric tetragonal phase ($P4mm$) attributed to softening of the Γ_{15} phonon mode [4,17,18]. Thus, further understanding of the vibrational characteristics is essential for elucidating the mechanisms behind their phase transitions.

Conventional methods of phonon analysis, such as neutron inelastic scattering or optical spectroscopies (infrared and Raman), have long served as valuable tools. In addition, recent advancements in monochromatic electron sources via electron energy-loss spectroscopy (EELS) in (scanning) transmission electron microscopy [(S)TEM] enable phonon excitation by taking the advantage of high spatial resolution [19]. While current limitations in the energy resolution of EELS may restrict its application to certain materials, such

*Contact author: haruta@eels.kuicr.kyoto-u.ac.jp

as ferroelectric transition metal materials, further developments in monochromatic electron sources are expected. On the other hand, the K edge in energy-loss near-edge structure (ELNES) and equivalent x-ray absorption near-edge structure (XANES) have been reported to reflect indirect vibrational information [20–27]. The origin of the K -edge prepeak of transition metals has been linked to the forbidden transition due to vibration-induced symmetry breaking [22–24]. Nemausat *et al.* demonstrated the significance of incorporating phonon effects using density functional theory (DFT) with harmonic approximation in simulating K edge [25,26]. These studies highlight that classical molecular dynamics serve as an alternative for considering anharmonic effects at high temperatures. Delhommaye *et al.* have also provided insights into thermal effects on multipole transitions and angular dependence in K edge [27]. Conversely, vibrational effects on the $L_{2,3}$ edge of transition metals have long been only simply treated as spectral broadening within semiempirical multiplet calculations [28]. Recently, our research reported the high sensitivity of thermal vibration effects in Ti $L_{2,3}$ -edge ELNES of cubic SrTiO₃, verified through cluster-based crystal field multiplet calculations incorporating vibration effects. The results indicated that only the atomic vibration of O significantly affects the spectral changes, while the effects from Ti and Sr vibrations are minimal. By leveraging this characteristic of distinct impacts, the anisotropic thermal vibration factors for oxygen in SrTiO₃ were successfully extracted by fitting experimental Ti $L_{2,3}$ -edge spectra with simulated spectra [29]. Additionally, this EELS approach offers the advantage of probing local regions, such as interfaces and surfaces, or samples that are challenging to synthesize in bulk form.

In the present study, we employ our previously reported ELNES approach combined with simulated spectra to conduct an in-depth exploration of the thermal vibration behavior of oxygen atoms within the cubic phase of PbTiO₃. This investigation involves a comparative analysis with cubic SrTiO₃, which shares an identical crystal structure and lattice constant at a different high temperature. Notably, while BaTiO₃ also exhibits a cubic phase above T_C , it has been discovered by electron microscopy studies that the presence of a local rhombohedral structure within all phases of BaTiO₃ [30] differs from the case of PbTiO₃ [31]. Our present research focuses exclusively on PbTiO₃ to avoid this potential confusion. Understanding these differences in the cubic paraelectric phase holds potential significance in predicting the types of low-temperature phase transition mechanisms in perovskites.

II. METHODS

A. Experimental details

EELS was conducted using a monochromated JEOL-ARM200F in STEM mode at a 200-kV acceleration voltage and a Gatan Quantum ERS spectrometer. The specimen was 99.5% PbTiO₃ powder from Furuchi Chemical Company, with a particle size of 300 mesh (<50 μm). EELS was acquired at a relative thickness (t/λ) of 0.4–0.6 (t and λ are the thickness and inelastic mean-free path, respectively). The specimen was heated from room temperature to 1073 K in a heating holder (JEOL, EM-31670SHTM). The probe

convergence semiangle was 32.6 mrad, and the EELS collection semiangle was 58.1 mrad. Incident electrons were monochromated using a 1.3- μm energy slit, and the spectra were measured at an energy dispersion of 0.025 eV/channel with a 0.125-eV practical energy resolution. The spectra were acquired in spectrum imaging mode in an area of about $50 \times 25 \text{ nm}^2$ under a short dwell time condition of 0.02 s to avoid irradiation damage, and 5000 spectra were accumulated after subtracting an ultra-high-quality dark reference and applying an optimized gain correction to improve signal-to-noise (S/N) ratio [32].

B. Calculation details

Simulated Ti $L_{2,3}$ -edge spectra were calculated by the crystal field multiplet calculation with atomic vibration effects incorporated in the original PYTHON code [29,52]. The calculation is implemented into the cluster-based program MULTIX [33], which only takes coordinates and charge of ions as input without any symmetry. The crystal field model provides an effective explanation in numerous instances despite a lack of consideration of the charge transfer effect [33,34]. Notably, the charge transfer effect has been reported to have a minor influence on the Ti $L_{2,3}$ edge in O_h symmetry [29], with negligible broadening of the L_3 edge and slight broadening of the L_2 edge. Moreover, the charge transfer effect would be smaller at higher temperatures due to the reduction in hybridization between the O $2p$ and Ti $3d$ states caused by volume expansion. A large deviation between the simulated and experimental L_2 -edge spectra was observed due to the omission of transitions to the $4s$ orbital or continuum states in the simulated spectra. Therefore, the analysis exclusively focuses on L_3 edge, where the scaling parameters (S_{Coulomb} , $S_{\text{so-coupling}}$, S_{xtal}) within the MULTIX program were adjusted to fit the experimental L_3 -edge spectra.

The cluster model for the MULTIX calculation was defined with a center on the metal site (Ti⁴⁺), extending to a 16- \AA cutoff radius determined by the spectral convergence [29]. The single crystal cluster included 1425 ions for SrTiO₃ and 1304 ions for PbTiO₃. In addition, atomic vibrations were incorporated into the calculation with displaced atomic positions [29,52] based on the frozen phonon approximation [35]. While a correlated vibration model would provide more realistic atomic movements, incorporating a simple Einstein model with uncorrelated atomic movement allowed our approach to retain thermal vibration factors (U) as free parameters. This flexibility enabled the spectrum to be simulated using reported U factors or to implement further fitting procedures. Each atomic displacement was generated by a Gaussian distribution function for which the standard deviation σ was set in accordance with the atomic mean square displacement $U = \sigma^2$ based on the harmonic oscillator approximation. Each displaced structure represents one of the frozen phonon configurations (FPCs) that can be seen as breaking from the original crystal symmetry. The calculation automatically repeated with N different frozen phonon configurations (FPCs) by the original PYTHON code. The average of N FPCs spectra constituted the final simulated spectrum. In this study, the final simulated spectra represented the average of 4000 FPC spectra.

TABLE I. Thermal vibration factors for cubic phase PbTiO_3 and SrTiO_3 .

Material	Method	Ref.	T (K)	a (Å)	$U_{\text{Pb/Sr}}$ (Å ²)	U_{Ti} (Å ²)	$U_{\text{O}(11)}$ (Å ²)	$U_{\text{O}(22)}$ (Å ²)
PbTiO_3	EELS ^a	present	1073				0.01 ± 0.002	0.01 ± 0.003
	EELS ^a	present	873				0.0097 ± 0.0025	0.0092 ± 0.003
	XRD ^a	[43]	873	3.9759	0.03782	0.01552	0.01442	0.0372
	SXRD ^a	[45]	873	3.9702	0.00424	0.01962	0.02012	0.02421
	SXRD/MEM ^b	[44]	850	3.97292	0.0382	0.0175	0.0125	0.0318
	neutron ^b	[46]	803	3.96881	0.0381	0.0170	0.0119	0.0289
SrTiO_3	theory ^c	[37]	1850	3.9702	0.02407	0.01068	0.01110	0.0360
	theory ^c	[37]	873	3.92898	0.01393	0.00631	0.00614	0.02040
	EELS ^a	[29]	873				0.0052 ± 0.002	0.0182 ± 0.003

^aSingle crystal.^bPowder.^cLattice constant and corresponding temperature are referenced from [38,45].

Our previous research demonstrated that the anisotropic oxygen thermal vibration factors of oxygen ($U_{\text{O}(11)}$ and $U_{\text{O}(22)}$) could be extracted from experimental ELNES spectra by fitting with simulated spectra [29]. In this study, the same procedure was employed to estimate the U_{O} values for PbTiO_3 at 873 and 1073 K in the cubic phase. The spectra were simulated with $U_{\text{O}(11)}$ and $U_{\text{O}(22)}$ set as free parameters, using a linear increase step of 0.0005 Å for $U_{\text{O}(11)}$ and 0.001 Å for $U_{\text{O}(22)}$. The effect of cation vibration can be neglected because only oxygen's vibration had a significant effect on the $L_{2,3}$ -edge spectral shape [29]. The optimal solution of anisotropic U_{O} is determined as the one with the minimal mean-square error (MSE) between the experimental and simulated spectra. The fitting energy range focuses on 456–461 eV in L_3 edge. At each temperature, three experimental spectra were used to estimate anisotropic U_{O} values, and the final estimated values were determined by averaging the optimal values from each spectrum.

Theoretical thermal vibration factors for SrTiO_3 were simulated by ALAMODE [36,37] for comparison (Table I). The crystal structure of SrTiO_3 at 1850 K [38] closely resembles that of PbTiO_3 at 873 K, with the only distinction being the A-site element. In addition, calculations for the density of states (DOS) and charge density map for cubic PbTiO_3 and SrTiO_3 were performed based on density functional theory (DFT) with the WIEN2K package [39], using the linearized augmented plane-wave (LAPW) method. The charge density was plotted by the program VESTA [40].

III. RESULTS AND DISCUSSION

Figure 1 shows the temperature dependence of PbTiO_3 Ti $L_{2,3}$ -edge ELNES spectra acquired at 293, 473, 673, 873, and 1073 K, where the paraelectric-ferroelectric phase transition of PbTiO_3 occurs at $T_{\text{C}} = 763$ K [7,41]. The experimental spectra show four main peaks roughly assigned to L_3 - t_{2g} , L_3 - e_g , L_2 - t_{2g} , and L_2 - e_g transitions based on crystal field theory coupled with a one-electron approximation. Four characteristic peaks resembling those found for the Ti $L_{2,3}$ edge of SrTiO_3 were observed in the paraelectric cubic phase (873 and 1073 K). However, asymmetric energy splitting of L_3 - e_g peaks was observed below T_{C} in the ferroelectric tetragonal phase. This spectral feature could not be reproduced in the present

simulation with the tetragonal structure model, likely due to the long-range band structure effect. Krüger reported that the L_3 - e_g peak splitting in rutile and anatase TiO_2 is primarily due to long-range band effects, while the local distortion of the TiO_6 octahedra only has a minor effect [42]. Given the complexities associated with the long-range effect in the tetragonal phase, we focus on the cubic phase that can be interpreted by the local crystal field multiplet effect in this study.

The oxygen thermal vibration factors for cubic PbTiO_3 were estimated from the experimental Ti $L_{2,3}$ -edge spectra using our previously reported fitting procedures [29]. Table I shows the estimated values at 873 and 1073 K. Oxygen

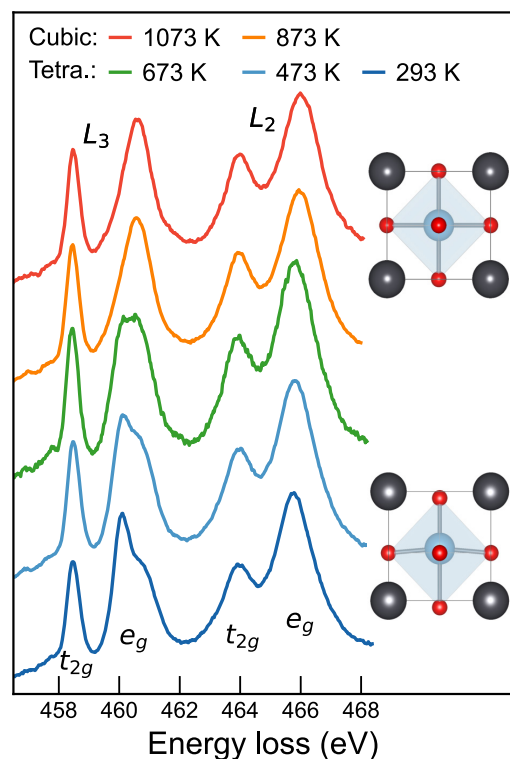


FIG. 1. Ti $L_{2,3}$ -edge spectra of PbTiO_3 obtained at 293, 473, 673, 873, 1073 K. The insets are the corresponding crystal structure of PbTiO_3 in cubic and tetragonal phases, respectively.

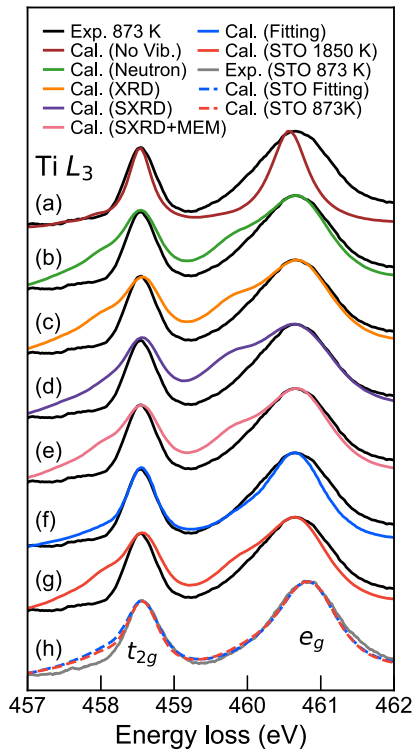


FIG. 2. Experimental (873 K, black) and simulated Ti L_3 edges for PbTiO₃. Spectra are simulated (a) without vibration effects, while others incorporate different thermal vibration factors (U) by (b)–(e) reported studies [43–46], (f) our estimation, and (g) theoretical SrTiO₃ at 1850 K. (h) The experimental (873 K, gray) and simulated Ti L_3 edges for SrTiO₃, where the U values derive from theoretical calculation (red, dashed) and our estimation (blue, dashed) [29]. U values used for simulation are shown in Table I.

vibrations in cubic PbTiO₃ exhibit relatively isotropic behavior. Thermal vibration factors for cubic PbTiO₃ have been reported in previous studies using single-crystal x-ray diffraction [43], powder synchrotron x-ray diffraction (SXRD) with the maximum entropy method (MEM) [10,44,45], and neutron powder diffraction [46] techniques. Previous investigations generally report anisotropic U_{O} values that are larger than those obtained in this study. The only exception is the single-crystal SXRD study [45], which shows relatively isotropic values, yet still exceeding our estimated values. The deviation of thermal vibration factors obtained from different diffraction methods (neutron or x ray) could be attributed to sample and particle size, whether bulk single crystal or powder. Generally, single crystal samples provided more accurate thermal vibration factor measurements compared to powder samples, as they reduce orientation effects and surface effects like oxidation and contamination. Estimation using the experimental $L_{2,3}$ -edge spectrum, with the advantage of local measurements, offers a complementary method to obtain partial thermal vibration factors regardless of sample size, even in local regions such as surfaces and interfaces.

Figure 2 shows comparisons between the experimental and simulated Ti L_3 -edge spectra using different thermal vibration factors (Table I) for PbTiO₃ around 873 K. The simulated spectrum without thermal vibration [Fig. 2(a)] exhibits a much

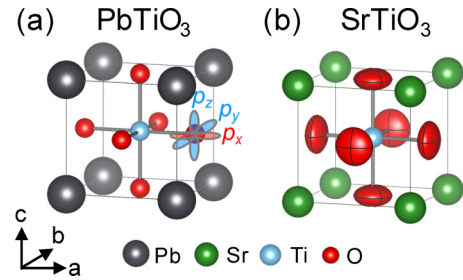


FIG. 3. Atomic vibration models (with 99% probability) of (a) PbTiO₃ at 873 K and (b) SrTiO₃ at 1850 K. Oxygen p orbitals marked at (0, 0.5, 0.5) were used in PDOS. The corresponding PDOS for oxygen p_y and p_z symmetries are identical but differ from p_x .

narrower broadening around the L_3 - e_g peak, showing the importance of incorporating the vibration effect into $L_{2,3}$ -edge simulation. The simulated spectrum [Fig. 2(f)] with optimized vibration factors by our spectral fitting demonstrates good agreement with the experimental spectrum. This validates that the atomic vibration contributed to the broadening effect of $L_{2,3}$ edge [28,29,52]. On the other hand, the simulated spectra [Figs. 2(b)–2(e)] using the U values determined by x-ray [43–45] and neutron diffraction experiments [46] exhibit a significant asymmetric broadening in the L_3 -edge region and fail to reproduce the experimental spectrum. The deviation of simulated spectra confirmed the high sensitivity of the Ti L_3 -edge spectrum to thermal vibration factors of oxygen. The anisotropic vibration factors of oxygen are more sensitive to measurement conditions in diffraction experiments, as oxygen’s light atomic mass results in a lower signal intensity from a smaller scattering cross section, and they are further influenced by oxidation and crystal imperfections. The successful reproduction of the experimental spectrum suggested a more isotropic oxygen vibration behavior in PbTiO₃.

For a comparative study of the isotropic/anisotropic vibration behavior, PbTiO₃ at 873 K and SrTiO₃ at 1850 K were selected, both possessing cubic perovskite structure with a lattice constant of 3.97 Å, and differing only in the A-site cations, Pb and Sr. Figure 3 and Table I show a comparison of the vibration factors for PbTiO₃ at 873 K and SrTiO₃ at 1850 K. While $U_{\text{O}(11)}$ has similar values for the two materials, $U_{\text{O}(22)}$ is significantly different. The pronounced anisotropy for oxygen vibration in cubic SrTiO₃ has been unveiled by several single-crystal diffraction experiments [47–50] and theoretical calculations [36,37], and such anisotropic models can well reproduce experimental $L_{2,3}$ -edge spectra [29]. Additionally, Fig. 2(h) shows previously reported experimental and simulated Ti L_3 edge of SrTiO₃ at 873 K [29], corresponding to anisotropic U values for simulation derived from theoretical calculation [37] and L_3 -edge fitting procedure estimates [29], respectively (Table I). The consistency observed in these spectra across a wide temperature range (300–1073 K) [29] validates the reliability of theoretical [37] anisotropic U values for high-temperature cubic SrTiO₃. Notably, the simulated spectrum with the theoretical anisotropic U values of SrTiO₃ at 1850 K [Fig. 2(g)] generated a shoulder peak at the low-energy side of the L_3 - e_g peak, which significantly deviates

from the experimental spectrum of PbTiO_3 at 873 K. However, such shoulder peaks on L_3 - e_g have been reported at both room temperature and 873 K in SrTiO_3 when the isotropic vibration model is assumed [52]. This contradiction suggests that the presence of the L_3 - e_g shoulder peak feature does not directly result from isotropy/anisotropy of oxygen vibrations, but is influenced by both the ratio and magnitude of $U_{O(11)}$ and $U_{O(22)}$ due to their unequal contribution to $L_{2,3}$ edge. Furthermore, a distinct difference in vibrational behavior between the two materials, despite their nearly identical crystal structures aside from the A -site cation, suggests that the A -site cation plays a crucial role in modifying the vibrational dynamics. Our finding aligns with the results reported by Kuroiwa *et al.* [8,51], which revealed an anisotropic distribution of oxygen in SrTiO_3 and an isotropic distribution in PbTiO_3 with experimental charge density maps obtained by MEM. Anisotropy of oxygen vibration in the perovskite structure was reported by Hewat with KNbO_3 [53,54]. This work attributed the anisotropy to low-frequency zone boundary vibrational modes, corresponding to rotations of oxygen octahedra, which are known to be unstable from lattice dynamical calculation [55]. Fabini *et al.* further provided strong evidence in CsSnBr_3 perovskite with x-ray and neutron diffraction, demonstrating that the large anisotropic vibration of Br anions in cubic phase ($Pm\bar{3}m$) is related to its dynamic octahedral rotations in a phase transition to tetragonal phase ($P4/m\bar{3}m$) [56]. Additionally, SrTiO_3 has been found to undergo a phase transition to the tetragonal phase with a rotation of oxygen octahedra below 110 K due to softening of the R_{25} phonon mode [2,14,15]. The anisotropic oxygen vibration in SrTiO_3 with a larger amplitude on the Sr-O plane ($U_{O(22)} \simeq 0.036 \text{ \AA}^2$), suggests a correlation of the unstable rotational vibration modes, which potentially account for the octahedral rotational phase transition due to softening of the R_{25} mode. In contrast, the coexistence of soft Γ_{15} and R_{25} phonon modes in cubic PbTiO_3 was reported by Tomeno *et al.* through a phonon dispersion analysis [57]. This combination of instability in zone-center and zone-boundary modes may lead to a relatively isotropic vibration of oxygen with a smaller $U_{O(22)}$ ($\simeq 0.009 \text{ \AA}^2$) in PbTiO_3 . This relatively isotropic vibration may imply a zone-center displacive phase transition in low temperature that differs from the SrTiO_3 one. Although our approach is unable to directly detect these phonon modes, we may discuss the potential phase transition mechanisms through the observed anisotropy/isotropy vibration of oxygen.

Finally, we further investigated the reason for isotropic oxygen thermal vibration in cubic PbTiO_3 from the point of view of the electronic structure. Thermal vibration in materials is affected by several factors, such as the crystal structure, chemical bonding, and atomic mass. Generally, the diverse material properties of perovskite transition metal (TM) oxides can be attributed to the variable valence states of TM $3d$ orbitals, which engage in strong hybridization with oxygen $2p$ orbitals, resulting in robust covalent bonding. Conversely, the A -site cation primarily influences crystal structure distortion, leading to alterations in the electronic structure of the B -site TM cation. Thus, the chemical bond between the A -site cation and oxygen has a relatively more ionic nature. Previous reports on the thermal vibration factors in SrTiO_3 [29,52] indicate smaller values for U_{Ti} and $U_{O(11)}$ across the entire

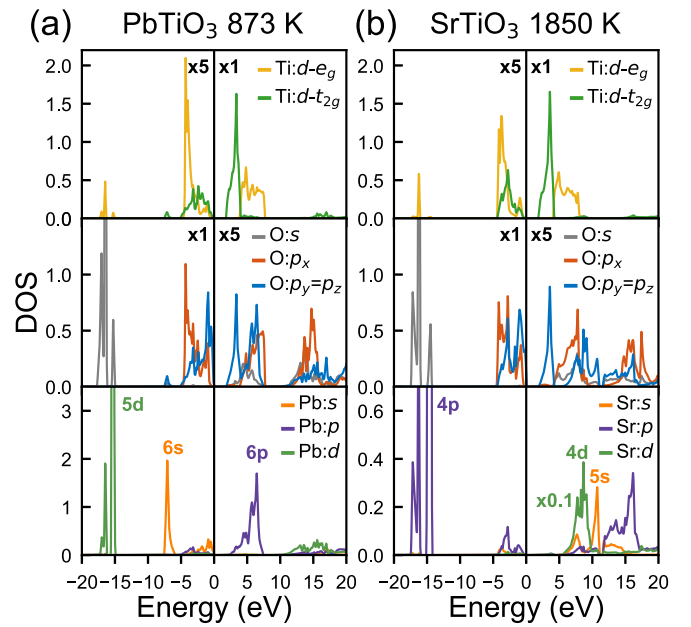


FIG. 4. Ground state PDOS of (a) PbTiO_3 at 873 K and (b) SrTiO_3 at 1850 K. The PDOS have been amplified for visual clarity.

temperature range, attributed to the strongly covalent Ti-O bond, whereas larger values of $U_{O(22)}$ and U_{Sr} are associated with a weaker ionic bond. Figure 4 shows the calculated partial density of states (PDOS) for cubic PbTiO_3 (873 K) and SrTiO_3 (1850 K). The oxygen position for the PDOS is defined as (0, 0.5, 0.5), as indicated in Fig. 3, resulting in an orbital with $p_x \neq p_y = p_z$. In the conduction band, the Ti $3d$ band exhibits crystal field splitting, separating into t_{2g} and e_g states, and hybridizes with the O $2p$ band, resulting in a small oxygen p DOS in the conduction band and a small Ti d DOS in the valence band. Although, in general, valence states composed of Ti $3d$ and O $2p$ states are considered for bond strength discussions, these states exhibit only small variations between these materials. This suggests comparable bond strengths between O and Ti in the two materials, reflected in the similar $U_{O(11)}$ values observed. On the other hand, examining the A -site cations, the lone pair $6s$ valence electrons of Pb^{2+} ($[\text{Xe}] 4f^{14} 5d^{10} 6s^2 6p^0$) [58] and the $4p$ valence electrons of Sr^{2+} ($[\text{Ar}] 3d^{10} 4s^2 4p^6 5s^0 4d^0$) show an ionic bonding character with the O $2p$ state. These findings align with previous reports on the charge density distribution obtained by SXR MEM, indicating the presence of ionic A-O bonds [8,10,51]. However, the A-O plane charge density map of the valence band ($-5 \sim 0 \text{ eV}$), presented in Fig. 5, reveals a broader electron density distribution in Pb^{2+} compared to Sr^{2+} . This broader distribution in PbTiO_3 potentially leads to increased electron repulsion between Pb and O, restricting the dynamic movement of oxygen. Consequently, this slight difference in electron distribution likely contributes to the observed smaller $U_{O(22)}$ vibration factor observed for PbTiO_3 .

IV. CONCLUSION

In summary, we estimated the thermal vibration factor for oxygen in cubic PbTiO_3 using an indirect approach

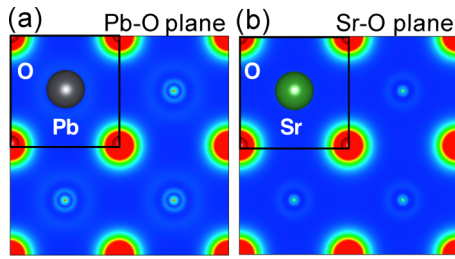


FIG. 5. Charge density map of A-O plane along [001] axis from valence band (energy range -5 to 0 eV) of (a) PbTiO_3 at 873 K and (b) SrTiO_3 at 1850 K, respectively.

of experimental Ti $L_{2,3}$ -edge EELS spectra combined with crystal field multiplet calculations considering the vibration effect. The results revealed that the oxygen vibrations in PbTiO_3 exhibit more isotropic behavior compared to previous diffraction-based values [43–46] which could not reproduce the experimental Ti $L_{2,3}$ -edge spectrum. In contrast, calculations for SrTiO_3 at 1850 K (same structure as PbTiO_3 at 873 K) displayed similar $U_{O(11)}$ values ($=0.01 \text{ \AA}^2$) but larger $U_{O(22)}$ ($=0.036 \text{ \AA}^2$). This anisotropy in SrTiO_3 is consistent with diffraction experiments at room temperature [47–50] and well reproduced the experimental Ti L_3 edge [29,52]. Based on the established relationship between the anisotropic oxygen vibration and the low-frequency octahedral rotations [53,54,56], the anisotropy in cubic SrTiO_3 suggested the association with the octahedral rotation type tetragonal phase transition at low temperatures triggered by the softening R_{25} phonon mode [2,14,15]. Conversely, the smaller $U_{O(22)}$ for PbTiO_3 suggests a possibly intrinsic small rotation mode, potentially related to a zone-center displacive-type phase transition due to the softening of the Γ_{15} mode without the rotation of octahedra. This research provides a potential means of

predicting the phase transition type for perovskites based on their thermal vibration factors in the high-temperature cubic phase. Further analysis of the distinct vibration behavior for the two materials was conducted by considering their bond properties through the DFT-calculated PDOS. Both materials exhibit similar covalent Ti-O bonds, resulting in comparable $U_{O(11)}$ values. On the other hand, Pb exhibits a broader electron density distribution in the valence band compared to Sr, leading to increased electron repulsion that restricts the vibrational amplitude of oxygen in the Pb-O plane ($U_{O(22)}$), thereby resulting in relative isotropic vibration behavior.

Given the sensitivity of oxygen's anisotropic vibration factors to experimental conditions, the present STEM-EELS (ELNES) approach aims to complement conventional diffraction-based measurement with its local measurement capabilities. With its inherent spatial resolution advantages, this approach is applicable to localized investigations regardless of sample size and can be extended to interface and surface analyses. While the use of a simplified uncorrelated vibration model limits our ability to directly resolve phonon mode, its flexibility allows us to retain thermal vibration factors (U) as variable and develop an approach to extract these factors from experimental $L_{2,3}$ edge. Our findings provide valuable insight into the phase transition related to the difference in vibration behavior in cubic perovskite of PbTiO_3 and SrTiO_3 . Future studies will aim to integrate correlated atomic vibration models, enabling a more realistic representation of atomic displacements and a thorough exploration of core-level spectroscopy associated with phonon modes.

ACKNOWLEDGMENT

This work was supported by JSPS KAKENHI Grant Number JP22H01956.

- [1] R. Ali and M. Yashima, Space group and crystal structure of the perovskite CaTiO_3 from 296 to 1720 K, *J. Solid State Chem.* **178**, 2867 (2005).
- [2] P. A. Fleury, J. F. Scott, and J. M. Worlock, Soft phonon modes and the 110 °K phase transition in SrTiO_3 , *Phys. Rev. Lett.* **21**, 16 (1968).
- [3] K. Sakayori, Y. Matsui, H. Abe, E. Nakamura, M. Kenmoku, T. Hara, D. Ishikawa, A. Kokubu, K. Hirota, and T. I. Takuro Ikeda, Curie temperature of BaTiO_3 , *Jpn. J. Appl. Phys.* **34**, 5443 (1995).
- [4] G. Shirane, J. D. Axe, J. Harada, and J. P. Remeika, Soft ferroelectric modes in lead titanate, *Phys. Rev. B* **2**, 155 (1970).
- [5] V. M. Goldschmidt, Die Gesetze der Kristallochemie, *Naturwissenschaften* **14**, 477 (1926).
- [6] R. E. Cohen, Origin of ferroelectricity in perovskite oxides, *Nature (London)* **358**, 136 (1992).
- [7] R. E. Cohen and H. Krakauer, Electronic structure studies of the differences in ferroelectric behavior of BaTiO_3 and PbTiO_3 , *Ferroelectrics* **136**, 65 (1992).
- [8] Y. Kuroiwa, S. Aoyagi, A. Sawada, J. Harada, E. Nishibori, M. Takata, and M. Sakata, Evidence for Pb-O covalency in tetragonal PbTiO_3 , *Phys. Rev. Lett.* **87**, 217601 (2001).
- [9] N. Choudhury, E. J. Walter, A. I. Kolesnikov, and C.-K. Loong, Large phonon band gap in SrTiO_3 and the vibrational signatures of ferroelectricity in ATiO_3 perovskites: First-principles lattice dynamics and inelastic neutron scattering, *Phys. Rev. B* **77**, 134111 (2008).
- [10] T. Abe, S. Kim, C. Moriyoshi, Y. Kitanaka, Y. Noguchi, H. Tanaka, and Y. Kuroiwa, Visualization of spontaneous electronic polarization in Pb ion of ferroelectric PbTiO_3 by synchrotron-radiation x-ray diffraction, *Appl. Phys. Lett.* **117**, 252905 (2020).
- [11] H. Lv, H. Gao, Y. Yang, and L. Liu, Density functional theory (DFT) investigation on the structure and electronic properties of the cubic perovskite PbTiO_3 , *Appl. Catal. A Gen.* **404**, 54 (2011).
- [12] M. F. M. Taib, M. K. Yaakob, O. H. Hassan, and M. Z. A. Yahya, Structural, electronic, and lattice dynamics of PbTiO_3 , SnTiO_3 , and SnZrO_3 : A comparative first-principles study, *Integr. Ferroelectr.* **142**, 119 (2013).
- [13] W. Cochran, Crystal stability and the theory of ferroelectricity, *Adv. Phys.* **9**, 387 (1960).

- [14] F. W. Lytle, X-ray diffractometry of low-temperature phase transformations in strontium titanate, *J. Appl. Phys.* **35**, 2212 (1964).
- [15] G. Shirane and Y. Yamada, Lattice-dynamical study of the 110 °K phase transition in SrTiO₃, *Phys. Rev.* **177**, 858 (1969).
- [16] K. A. Müller and H. Burkard, SrTiO₃: An intrinsic quantum paraelectric below 4 K, *Phys. Rev. B* **19**, 3593 (1979).
- [17] J. Harada, J. D. Axe, and G. Shirane, Neutron-scattering study of soft modes in cubic BaTiO₃, *Phys. Rev. B* **4**, 155 (1971).
- [18] G. Shirane, B. C. Frazer, V. J. Minkiewicz, J. A. Leake, and A. Linz, Soft optic modes in barium titanate, *Phys. Rev. Lett.* **19**, 234 (1967).
- [19] O. L. Krivanek, T. C. Lovejoy, N. Dellby, T. Aoki, R. W. Carpenter, P. Rez, E. Soignard, J. Zhu, P. E. Batson, M. J. Lagos, R. F. Egerton and P. A. Crozier, Vibrational spectroscopy in the electron microscope, *Nature (London)* **514**, 209 (2014).
- [20] Y. Matsui, K. Seki, A. Hibara, and T. Mizoguchi, An estimation of molecular dynamic behaviour in a liquid using core-loss spectroscopy, *Sci. Rep.* **3**, 1 (2013).
- [21] H. Katsukura, T. Miyata, M. Shirai, H. Matsumoto, and T. Mizoguchi, Estimation of the molecular vibration of gases using electron microscopy, *Sci. Rep.* **7**, 1 (2017).
- [22] D. Manuel, D. Cabaret, C. Brouder, P. Sainctavit, A. Bordage, and N. Trcera, Experimental evidence of thermal fluctuations on the x-ray absorption near-edge structure at the aluminum *K* edge, *Phys. Rev. B* **85**, 224108 (2012).
- [23] D. Cabaret and C. Brouder, Origin of the pre-edge structure at the Al *K*-Edge: The role of atomic vibrations, *J. Phys. Conf. Ser.* **190**, 012003 (2009).
- [24] C. Brouder D. Cabaret, A. Juhin, and P. Sainctavit, Effect of atomic vibrations on the x-ray absorption spectra at the *K* Edge of Al in α -Al₂O₃ and of Ti in TiO₂ rutile, *Phys. Rev. B* **81**, 115125 (2010).
- [25] R. Nemausat, D. Cabaret, C. Gervais, C. Brouder, N. Trcera, A. Bordage, I. Errea, and F. Mauri, Phonon effects on x-ray absorption and nuclear magnetic resonance spectroscopies, *Phys. Rev. B* **92**, 144310 (2015).
- [26] R. Nemausat, C. Gervais, C. Brouder, N. Trcera, A. Bordage, C. Coelho-Diogo, P. Florian, A. Rakhmatullin, I. Errea, L. Paulatto, M. Lazzeri, and D. Cabaret, Temperature dependence of x-ray absorption and nuclear magnetic resonance spectra: Probing quantum vibrations of light elements in oxides, *Phys. Chem. Chem. Phys.* **19**, 6246 (2017).
- [27] S. Delhommaye, G. Radtke, Ch. Brouder, S. P. Collins, S. Huotari, Ch. Sahle, M. Lazzeri, L. Paulatto, and D. Cabaret, Assessing temperature effects on multipole contributions and angular dependence in core-level spectroscopies, *Phys. Rev. B* **104**, 024302 (2021).
- [28] F. M. F. De Groot, J. C. Fuggle, B. T. Thole, and A. G., Sawatzky, *2p* x-ray absorption of *3d* transition-metal compounds: An atomic multiplet description including the crystal field, *Phys. Rev. B* **42**, 5459 (1990).
- [29] I.-C. Lin, M. Haruta, T. Nemoto, M. Goto, Y. Shimakawa, and H. Kurata, Extraction of anisotropic thermal vibration factors for oxygen from the Ti *L*_{2,3}-edge in SrTiO₃, *J. Phys. Chem. C* **127**, 17802 (2023).
- [30] K. Tsuda, R. Sano, and M. Tanaka, Nanoscale local structures of rhombohedral symmetry in the orthorhombic and tetragonal phases of BaTiO₃ studied by convergent-beam electron diffraction, *Phys. Rev. B* **86**, 214106 (2012).
- [31] K. Tsuda and M. Tanaka, Convergent-beam electron diffraction study of the local structure of the tetragonal phase of PbTiO₃, *Appl. Phys. Express* **6**, 101501 (2013).
- [32] M. Haruta, Y. Fujiyoshi, T. Nemoto, A. Ishizuka, K. Ishizuka, and H. Kurata, Extremely low count detection for EELS spectrum imaging by reducing CCD read-out noise, *Ultramicroscopy* **207**, 112827 (2019).
- [33] A. Uldry, F. Vernay, and B. Delley, Systematic computation of crystal-field multiplets for x-ray core spectroscopies, *Phys. Rev. B* **85**, 125133 (2012).
- [34] F. M. F. De Groot, Multiplet effects in x-ray spectroscopy, *Coord. Chem. Rev.* **249**, 31 (2005).
- [35] R. F. Loane, P. Xu, and J. Silcox, Thermal vibrations in convergent-beam electron diffraction, *Acta Crystallogr., Sect. A: Found. Crystallogr.* **47**, 267 (1991).
- [36] T. Tadano, Y. Gohda, and S. Tsuneyuki, Anharmonic force constants extracted from first-principles molecular dynamics: Applications to heat transfer simulations, *J. Phys.: Condens. Matter* **26**, 225402 (2014).
- [37] T. Tadano and S. Tsuneyuki, Self-consistent phonon calculations of lattice dynamical properties in cubic SrTiO₃ with first-principles anharmonic force constants, *Phys. Rev. B* **92**, 054301 (2015).
- [38] D. de Ligny and P. Richet, High-temperature heat capacity and thermal expansion of SrTiO₃ and SrZrO₃ perovskites, *Phys. Rev. B* **53**, 3013 (1996).
- [39] K. Schwarz and P. Blaha, Solid state calculations using WIEN2K, *Comput. Mater. Sci.* **28**, 259 (2003).
- [40] K. Momma and F. Izumi, VESTA 3 for three-dimensional visualization of crystal, volumetric and morphology data, *J. Appl. Crystallogr.* **44**, 1272 (2011).
- [41] S. A. Mabud and A. M. Glazer, Lattice parameters and birefringence in PbTiO₃ single crystals, *J. Appl. Crystallogr.* **12**, 49 (1979).
- [42] P. Krüger, Multichannel multiple scattering calculation of *L*_{2,3}-edge spectra of TiO₂ and SrTiO₃: Importance of multiplet coupling and band structure, *Phys. Rev. B* **81**, 125121 (2010).
- [43] J. Kwapuliński, J. Kusz, H. Böhm, and J. Dec, Thermal vibrations in PbTiO₃ single crystals, *J. Phys.: Condens. Matter* **17**, 1825 (2005).
- [44] Y. Terado, C. Moriyoshi, Y. Kuroiwa, Y. Yamamura, and M. Iwata, Relationship between MPB and emergence of structural boundary in cubic phase of Pb-based perovskite-type solid solutions PZT and PZN-PT, *Trans. Mater. Res. Soc. Jpn.* **33**, 47 (2008).
- [45] A. Yoshiasa, T. Nakatani, A. Nakatsuka, M. Okube, K. Sugiyama, and T. Mashimo, High-temperature single-crystal x-ray diffraction study of tetragonal and cubic perovskite-type PbTiO₃ phases, *Acta Crystallogr. Sect. B: Struct. Sci. Cryst. Eng. Mater.* **72**, 381 (2016).
- [46] N. Zhang, H. Yokota, A. M. Glazer, and P. A. Thomas, The not so simple cubic structure of PbZr_{1-x}Ti_xO₃ (PZT): Complex local structural effects in perovskites, *Acta Crystallogr., Sect. B: Struct. Sci., Cryst. Eng. Mater.* **67**, 461 (2011).
- [47] W. Jauch and M. Reehuis, Electron-density distribution in cubic SrTiO₃: A comparative gamma-ray diffraction study, *Acta Crystallogr., Sect. A: Found. Crystallogr.* **61**, 411 (2005).
- [48] E. N. Maslen, N. Spadaccini, T. Ito, F. Marumo, and Y. Satow, A synchrotron radiation study of strontium titanate,

- Acta Crystallogr., Sect. B: Struct. Sci., Cryst. Eng. Mater.* **51**, 939 (1995).
- [49] Y. A. Abramov, V. G. Tsirelson, V. E. Zavodnik, S. A. Ivanov, and I. D. Brown, The chemical bond and atomic displacements in SrTiO₃ from x-ray diffraction analysis, *Acta Crystallogr., Sect. B: Struct. Sci., Cryst. Eng. Mater.* **51**, 942 (1995).
- [50] R. J. Nelmes, G. M. Meyer, and J. Hutton, Thermal motion in SrTiO₃ at room temperature: Anharmonic or disordered? *Ferroelectrics* **21**, 461 (1978).
- [51] Y. Kuroiwa, S. Aoyagi, A. Sawada, E. Nishibori, M. Takata, M. Sakata, H. Tanaka, and J. Harada, Atomic replacement effect on electron charge density of perovskite oxides, *J. Korean Phys. Soc.* **42**, 1425 (2003).
- [52] M. Haruta, T. Nemoto, and H. Kurata, Sub-picometer sensitivity and effect of anisotropic atomic vibrations on Ti *L*_{2,3}-edge spectrum of SrTiO₃, *Appl. Phys. Lett.* **119**, 232901 (2021).
- [53] A. W. Hewat, Cubic-tetragonal-orthorhombic-rhombohedral ferroelectric transitions in perovskite potassium niobate: Neutron powder profile refinement of the structures, *J. Phys. C: Solid State Phys.* **6**, 2559 (1973).
- [54] A. W. Hewat, Low frequency zone boundary modes in perovskite ferroelectrics indicated by anisotropic Debye-Waller factors, *Phys. Status Solidi B* **53**, K33 (1972).
- [55] R. A. Cowley, Lattice dynamics and phase transitions of strontium titanate, *Phys. Rev.* **134**, A981 (1964).
- [56] D. H. Fabini, G. Laurita, J. S. Bechtel, C. C. Stoumpos, H. A. Evans, A. G. Kontos, Y. S. Raptis, P. Falaras, A. Van der Ven, M. G. Kanatzidis, and R. Seshadri, Dynamic stereochemical activity of the Sn²⁺ lone pair in perovskite CsSnBr₃, *J. Am. Chem. Soc.* **138**, 11820 (2016).
- [57] I. Tomeno, J. A. Fernandez-Baca, K. J. Marty, K. Oka, and Y. Tsunoda, Simultaneous softening of acoustic and optical modes in cubic PbTiO₃, *Phys. Rev. B* **86**, 134306 (2012).
- [58] H. M. H. Miyazawa, E. N. E. Natori, S. M. S. Miyashita, T. S. T. Shimoda, F. I. F. Ishii, and T. O. T. Oguchi, Electronic states of perovskite-type oxides and ferroelectricity, *Jpn. J. Appl. Phys.* **39**, 5679 (2000).